




Optimizing Microstructure and Mechanical Properties of Cold-Rolled Medium-Mn Steel Through Intercritical Annealing and Warm Rolling

RANJIT KUMAR,¹ AVANISH KUMAR CHANDAN,^{2,3}
GAURAV KUMAR BANSAL,^{2,3} SUMIT K. SHARMA,¹
and KIRTY MADHAVI ^{1,4}

1.—Department of Metallurgical Engineering, B.I.T Sindri, Dhanbad 828123, India. 2.—Materials Engineering Division, National Metallurgical Laboratory CSIR, Jamshedpur 831007, India. 3.—Academy of Scientific and Innovative Research (AcSIR), Ghaziabad 201002, India. 4.—e-mail: kirtymadhavi.met@bitsindri.ac.in

This study investigates the influence of intercritical annealing (IA) and warm-rolling (WR) parameters on the microstructure and mechanical properties of a cold-rolled medium-Mn steel (CR-MMnS). IA was conducted between temperatures of 620°C and 740°C, while warm rolling was carried out after IA to improve mechanical properties. To calculate the parameters for the IA and IA + WR treatments, thermodynamic model calculations were conducted using the ThermoCalc database, TCFE9. The microstructural analysis of CR-MMnS revealed that IA promoted the formation of globular morphology of ferrite/martensite and retained austenite along with the formation of carbides, while warm rolling resulted in refined grain sizes and the breakup of coarser carbides with lamellar morphology. Mechanical testing demonstrated that the combination of intercritical annealing and warm rolling (IA + WR) achieved improved tensile strength and yield strength compared to the individual intercritical annealing. The findings provide valuable insights into the optimization of intercritical annealing and warm-rolling parameters for enhancing microstructure and mechanical properties in medium-Mn steel. This research contributes to the development of advanced steel materials with enhanced performance for various engineering applications.

INTRODUCTION

Recent research has shown that medium manganese (Mn) steel retaining 15–30% austenite exhibited excellent mechanical properties and versatility.¹ Medium-Mn steel is a type of advanced high-strength steel (AHSS) that has Mn content between 3% and 12% by weight;² the mechanical properties of MMS surpass those of the 1st-Gen AHSS and it has potentially lower cost than high Mn twinning-induced plasticity (TWIP) steel, making it a strong candidate for the 3rd-Gen AHSS. Miller³ first proposed such steel in the 1970s, but it

has gained a great deal of attention only recently (in the early 2010s) because steel has become increasingly important to many different industries, particularly the automobile industry, because of its favorable material cost-tensile property balance. Increasing the amount of Mn content in medium-Mn steel enhances the ability to retain austenite and its stability, which can be tailored through different heat treatment processes.⁴ Intercritical annealing and warm-rolling parameters play a role in achieving stable retained austenite, contributing to improved strength and ductility through TRIP and TWIP work-hardening mechanisms.⁵ Researchers are investigating the microstructure and mechanical attributes of medium-Mn steel and aiming to tailor its properties for specific applications. This steel resolves the strength–ductility

(Received May 16, 2024; accepted August 19, 2024)

trade-off seen in previous AHSS generations by embedding martensite/ferrite laths with austenite films. Carbon and manganese stabilize the austenite phase, with typical carbon content ranging from 0.2% to 0.4% in retained austenite, and intercritical annealing is employed for austenite reverted transformation (ART). Medium manganese steel aligns with the automotive industry's focus on lightweight construction for improved fuel efficiency and reduced carbon footprint while meeting structural integrity and crashworthiness requirements. The current focus of research on medium-Mn steels is mainly on the improvement of tensile properties, such as yield strength (YS), ultimate strength (UTS) and strength–ductility balance.⁶ Outstanding tensile properties that either meet or even surpass the required property have often been recorded in banana diagrams for such steels, as shown in Fig. 1.

Such steels have been reported to exhibit a high product of tensile strength and total elongation (~ 70),⁸ but certain characteristics remain poorly understood, including the microstructural evolution during processing stages and the optimization of alloying element's impact on microstructure and mechanical behavior. These steels typically undergo hot rolling, followed by cold rolling and intercritical annealing (IA) in which IA produces ferrite, retained austenite and martensite, which are optimal for the steel, but this results in reduced strength and increased ductility due to the introduction of ferrite upon cooling. Nowadays, several researchers have shown warm rolling following intercritical annealing (IA + WR) as an effective method to improve mechanical properties, particularly the yield strength.⁹ Warm rolling has gained popularity due to its potential advantages, as it eliminates certain steps in the processing of medium-Mn steel. As per the research reports, the warm rolling can refine the microstructure and harden the steel, resulting in increased strength while retaining ductility.¹⁰ Additionally, this process generates a large volume fraction of optimally stable austenite

in the final product. Further research is necessary to investigate the impact of intercritical annealing and warm-rolling parameters on the microstructure and mechanical properties of medium Mn steel. The objective of this study is to enhance our understanding of the phase transformation behavior of medium-Mn steels during the annealing and rolling processes, with specific emphasis on maximizing the amount of retained austenite. Additionally, this research aims to evaluate the mechanical properties of the medium-Mn steel and establish correlations between these properties and the microstructure.

EXPERIMENTAL DETAILS AND METHOD

In this work, the steel was prepared in an air induction furnace and cast into an ingot with 100 mm \times 100 mm cross section. The ingots were homogenized at 1250°C for 4 h followed by forging. The forged slabs were solution annealed at 1200°C for 2 h, followed by hot rolling up to a thickness of 5.5 mm, involving seven passes. The hot-rolled MMnS sheets underwent a softening treatment at 600°C for 4 h. The hot-rolled plate was then cold rolled to 2.5 mm, resulting in a 54.54% reduction. The medium-Mn steel had a chemical composition of 0.22 wt.% C, 5.2 wt.% Mn, 0.54 wt.% Al, 0.80 wt.% Si, 0.0054 wt.% P, 0.005 wt.% S and balanced Fe.

To establish an appropriate heat treatment and processing route schedule, the critical temperatures of Ae1 and Ae3 of the experimental steel obtained by ThermoCalc software were 530°C and 770°C, respectively. The cold-rolled sheets of 2.5 mm were subjected to intercritical annealing and warm-rolling heat treatment, as discussed in the introduction section. During intercritical annealing, the steels were soaked in a high-temperature furnace at 620°C, 660°C, 700°C, and 740°C for 30 min and then immediately quenched in water. Another set of cold-rolled samples underwent warm-rolling post-intercritical annealing at different temperatures. The intercritical annealing (IA) samples with the highest product of tensile strength and ductility, at temperatures of 660°C and 700°C, are selected for warm rolling. This is done to optimize the maximum volume fraction of RA, which will assist in enhancing the mechanical properties of medium-Mn steel through a low-temperature warm-rolling treatment. This method is designed to compare favorably with previous studies employing warm rolling at higher temperatures.

Specimens of 6 mm width and 25 mm gauge length were subjected to tensile tests using a universal testing machine at a constant crosshead velocity of 0.5 mm/min at room temperature. The microstructural examination was carried out using a scanning electron microscope (SEM) and electron backscattered diffraction (EBSD). Austenite volume fraction was determined by X-ray diffraction (XRD) based on the integrated intensities of austenite and ferrite diffraction peaks.

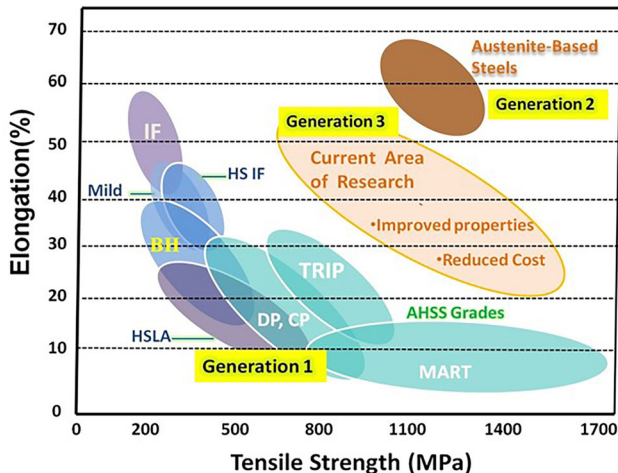


Fig. 1. Tensile properties of different groups of AHSS.⁷

THERMODYNAMIC PREDICTION

Thermodynamic predictions are crucial for predicting the retained austenite (RA) volume fraction during intercritical annealing (IA) treatments. Moor et al. developed a thermodynamic model to predict the optimal IA temperature and austenite amount and composition.¹¹

Figure 2a presents the variation of the equilibrium fraction of austenite with temperature. As the temperature increases, the presence of austenite also increases. This trend continues until reaching a temperature of 770°C, which corresponds to the Ae3 temperature where the microstructure becomes fully austenitic. Beyond this point, at a temperature of 1436.96°C, the fraction of austenite begins to decrease until reaching zero at 1465.20°C. The intercritical austenite composition also varies with annealing temperature. Manganese (Mn) and carbon (C) enrichment in austenite during IA aids in RA retention post-quenching. RA fraction estimation involves calculation of martensite start temperature (M_s) varying as a function of intercritical annealing temperature as per Eq. 1 proposed by Mahieu et al.¹²

$$M_s (\text{°C}) = 539 - 423(\%C) - 30.4(\%Mn) - 7.5(\%Si) + 30(\%Al) \quad (1)$$

The volume fraction of intercritical austenite, which would be athermally transformed into martensite after quenching to room temperature, can be determined using the empirical equation proposed by Koistinen and Marburger.¹³ Equation 2 is given as:

$$f_{\alpha'} = 1 - e^{-0.011(M_s - Q_T)} \quad (2)$$

where $f_{\alpha'}$ = volume fraction of freshly formed martensite; M_s = martensitic start temperature; Q_T = final quenching temperature (room temperature in the present case)

By subtracting this amount of freshly formed martensite from the equilibrium intercritical austenite fraction, the final retained austenite fraction in the microstructure at room temperature is obtained. Figure 2b presents the variation of predicted RA with the IA temperature. The maximum amount of RA can be stabilized in the samples intercritically annealed at 660°C.

HEAT TREATMENT SCHEDULE

The IA process involves annealing at temperatures ranging from 620°C to 740°C for 30 min followed by water quenching. IA + WR specimens are processed by quenching from 660°C to 700°C annealing temperatures in a salt bath maintained at 320°C and 375°C for a holding period of 80 s and 40 s, respectively, before being water quenched. Figure 3a provides a schematic of the IA process, while Fig. 3b illustrates the flowchart for the IA + WR process.

Warm rolling post-IA at 660°C and 700°C impacts RA stability. Warm-rolling temperature choice relies on Md_{30} temperature, preventing martensitic transformation. Md_{30} is the temperature where half of the austenite (50%) transforms to martensite with 30% strain in uniaxial tension. Md_{30} is calculated from C, Mn, Si, and Al compositions and austenite grain size using Eq. 3.¹⁴

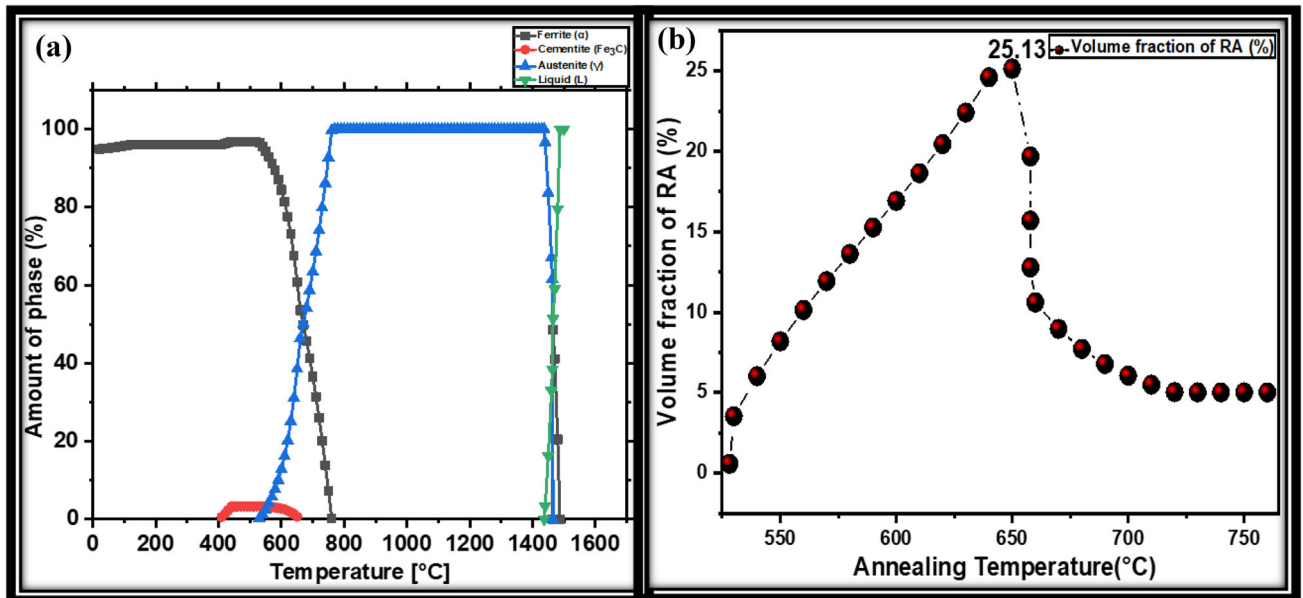


Fig. 2. (a) Phase fraction (%) as a function of temperature calculated based on thermo-calc for the steel under investigation. (b) Predicted variation of RA with IA temperature.

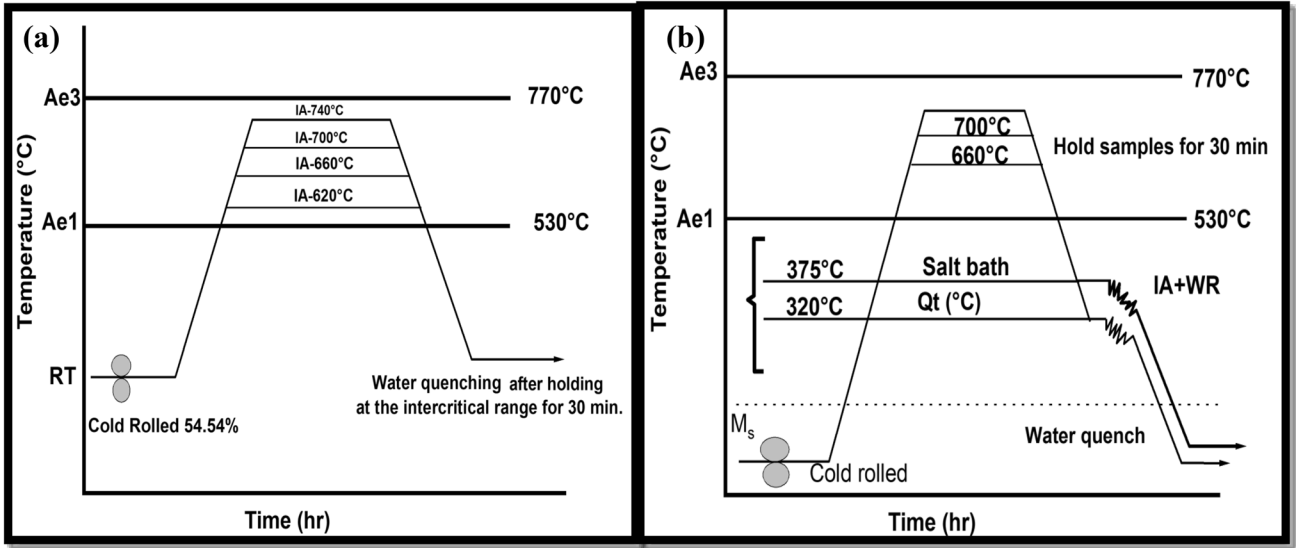


Fig. 3. (a) Schematic diagram for the IA process, (b) flowchart of IA + WR process.

$$\begin{aligned} \text{Md}_{30} = & 551 - 462(\%C) - 8.1(\%Mn) - 9.2(\%Si) \\ & - 1.42 * (-3.29 - 6.64 \log_{10} * d\gamma - 8) \end{aligned} \quad (3)$$

where compositions are given in wt.% and $d\gamma$ is the austenite grain size in μm .

The EBSD procedure for calculating grain size involved using the ImageJ software for scanning multiple sites across the sample surface. Specifically, a total of ten sites and eight sites were scanned for 660°C and 700°C samples. Each site covered an area of approximately $0.45 \mu\text{m}^2$ and $0.25 \mu\text{m}^2$, respectively. The grain size was calculated based on these scans, and the standard deviation (stdev) of the grain size measurements was found to be $0.31 \mu\text{m}$ and $0.11 \mu\text{m}$ for the 660°C and 700°C samples, respectively. This detailed analysis ensures the reliability and statistical significance of the grain size results obtained at the magnification used. The austenite grain size was obtained from the EBSD image quality as shown in Fig. 4.

Warm-rolling temperature selection aims to avoid excessive austenite to martensite transformation, guided by Md_{30} temperature. Holding duration at the quenching temperature prevents austenite decomposition. This was chosen based on the TTT diagram of the intercritical austenite phase generated from the JmatPro software (Table I).

RESULT AND DISCUSSION

Microstructure Characterization

Microstructure of Cold-Rolled Medium-Mn Steel

The initial microstructure of the as-received sample, which underwent cold rolling up to approximately 54.54%, was challenging to analyze using optical microscopy because of the high level of

deformation and low resolution of the technique (Fig. 5a). However, further investigation using scanning electron microscopy (SEM) and electron backscatter diffraction (EBSD) revealed that the microstructure in the cold-rolled state mainly consisted of deformed martensite. Notably, there was no presence of austenite or precipitates before intercritical annealing (Fig. 5b). EBSD phase mapping confirmed that the primary constituent of the microstructure was the body-centered cubic (BCC) phase, namely martensite/ferrite, with a very small fraction of retained austenite phase (Fig. 5c). The findings from EBSD were supported by X-ray diffraction (XRD) analysis, as only a few small peaks of the epsilon martensite (ϵ -martensite) phase were observed in addition to the main BCC phase (Fig. 5d). The formation of ϵ -martensite can be attributed to the presence of manganese content, which lowers the stacking fault energy (SFE) at room temperature.

Microstructure of IA and IA + WR Samples

Figure 6 displays the microstructure of the studied medium-Mn steel in IA and IA + WR states examined by SEM. The IA specimen annealed at 620°C led to the recrystallization and grain growth of the deformed grains produced during cold rolling. The occurrence of recrystallization was responsible for morphology difference in medium-Mn steel annealed at different temperature. With the increased annealing temperature, the grain morphology changed from mostly lamellar in the 620°C IA sample to fully globular in the 740°C IA sample (SEM micrographs). On the other hand, the WR samples exhibit a more deformed microstructure compared to the IA samples after salt bath and have a more deformed microstructure compared with the IA samples. The microstructural constituents

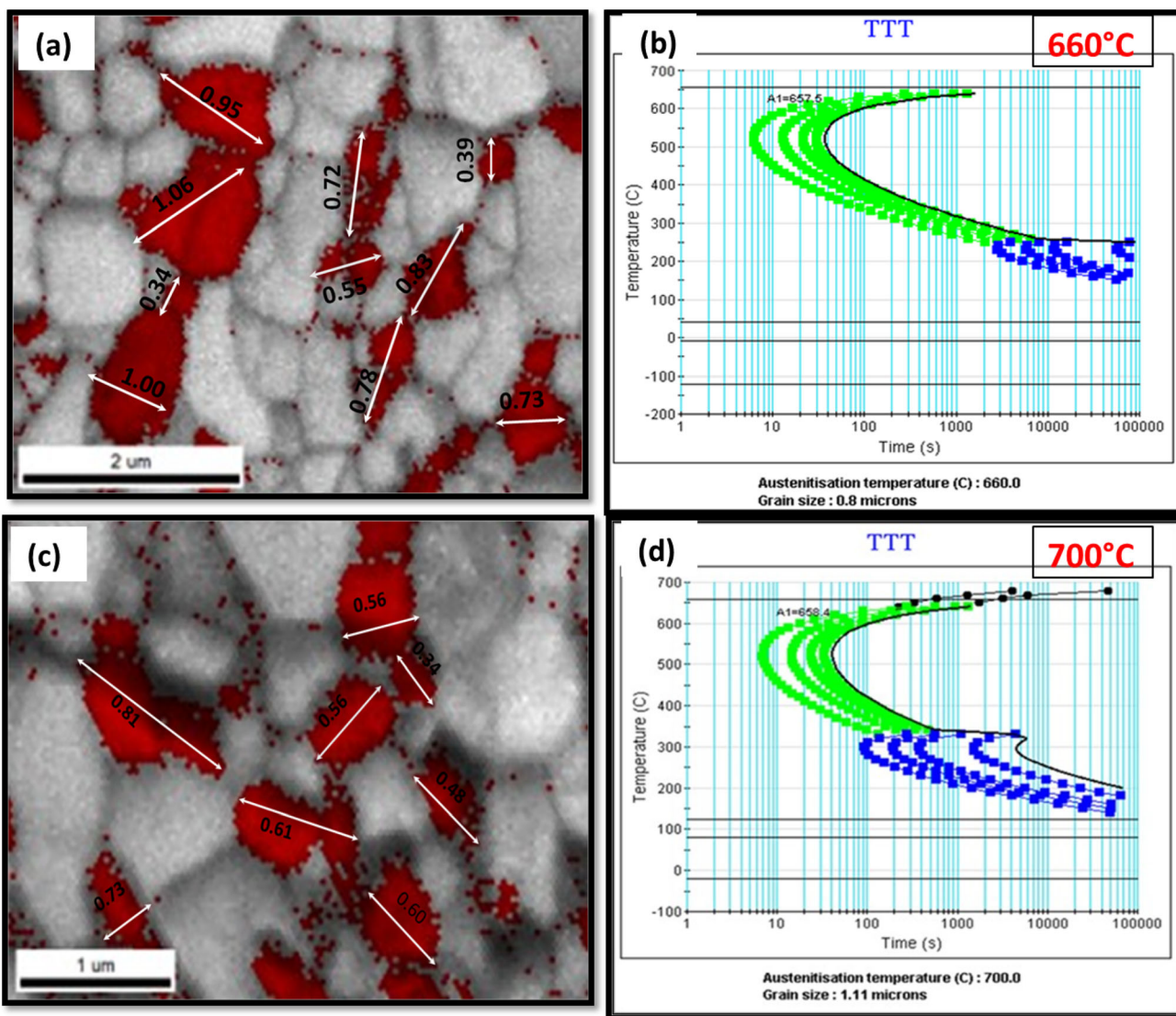


Fig. 4. Quenching time and temperature of specimens at different temperatures using JmatPro software, with a magnification of $\times 500$ for both samples: (a, b) IA—660°C—0.8 μ avg. GS. (c, d) IA—700°C—1.11 μ avg. GS.

Table I. Ms and Md₃₀ temperature of cold-rolled samples at different temperatures with their quenching temperature and time

| Composition and parameters | Temp. (°C) | |
|----------------------------|------------|-------|
| | 660°C | 700°C |
| Fe | 89.84 | 91.65 |
| C | 0.47 | 0.34 |
| Mn | 8.54 | 6.82 |
| AL | 0.22 | 0.28 |
| Si | 0.92 | 0.89 |
| G.S from EBSD (μ) | 0.8 | 1.11 |
| Ms (°C) | 80.8 | 187.7 |
| Md ₃₀ (°C) | 271.8 | 344.9 |
| QT (°C) | 320 | 375 |
| Qt (s) | 80 | 40 |

included elongated retained austenite and ferrite as the dominant phase after salt bath quenching at different temperature and time, followed by warm deformation. Moreover, it is obvious that the microstructure becomes finer with increasing warm-rolling deformation.

To analyze the microstructure in detail, EBSD was employed regarding the phase distribution as presented in Figs. 7 and 8 for the IA and IA + WR samples, respectively. Phase maps revealed a microstructure comprising ferrite (BCC) and austenite (FCC) after annealing, followed by water quenching. Notably, retained austenite displayed a globular morphology across all samples, except in IA-660°C sample. Actually, the interconnected globules of different phases resembled a lamellar structure under high magnification of SEM in the IA-660°C sample. This observation was consistent with

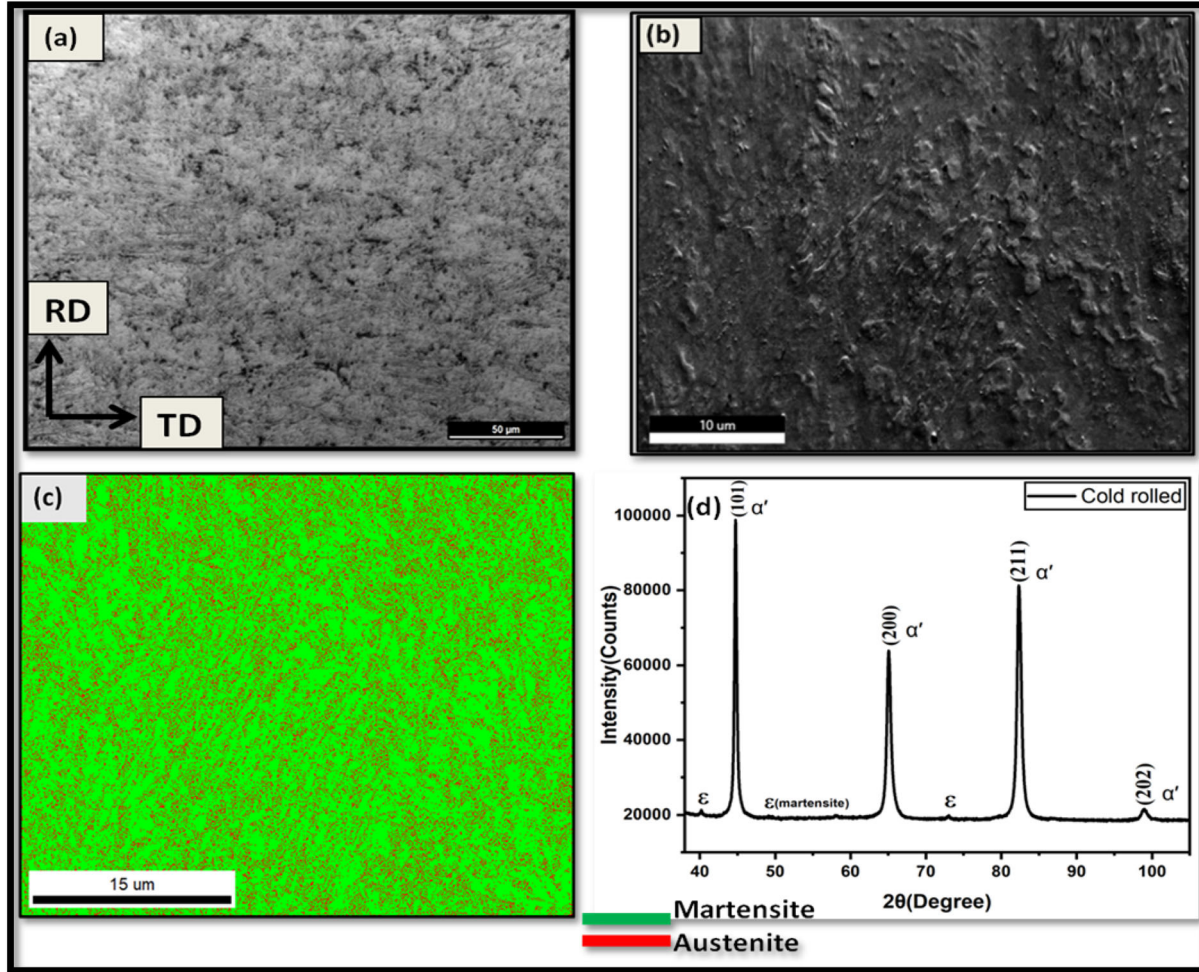


Fig. 5. Microstructure of cold-rolled medium-Mn steel: (a) optical image, (b) SEM image, (c) EBSD phase map, (d) XRD pattern.

SEM micrographs, illustrating the globular morphology of the constituent phase. In addition, the microstructure of both IA and IA + WR samples showed different amounts of austenite content. Figures 7 and 8 show that the grains of the retained austenite phase are located in the boundary regions of the ferrite and martensite phases. The volume fraction of retained austenite was 7%, 20%, 17%, and 9% calculated from EBSD map in the sample subjected to intercritical annealing at 620°C, 660°C, 700°C, and 740°C, respectively. These variations in retained austenite content can be attributed to the changes in the phase transformation kinetics and stability of the austenite phase at different annealing temperatures. In contrast to the IA samples, the IA + WR samples were warm rolled at 320°C and 375°C; a microstructure with a lamellar morphology is observed along with around 9% retained austenite content. This lamellar morphology is likely the result of the deformation and recrystallization processes that occurred during the warm-rolling step.

Phase Fraction Estimation Through XRD

Figure 9a shows the XRD peaks obtained at different intercritical annealing temperatures. The graphical representation indicates that the height of the austenite peaks progressively increases as the annealing temperature rises, suggesting a phenomenon called austenite reversion. This occurs after intercritical annealing, as evidenced by the appearance of FCC structure (γ) peaks in the XRD profiles. Notably, the peak intensity (height) increases only up to 700°C, after which it levels off, suggesting that approximately 700°C may serve as the optimal temperature for medium Mn steel. However, above 700°C, grain growth becomes the dominant mechanism, leading to the introduction of new defects and distortion at grain boundaries. Consequently, any further increase in peak intensities is hindered. It can be inferred that grain growth at higher temperatures impedes the desired improvement in peak intensities and ultimately affects the material's properties. Figure 9b shows

Optimizing Microstructure and Mechanical Properties of Cold-Rolled Medium-Mn Steel Through Intercritical Annealing and Warm Rolling

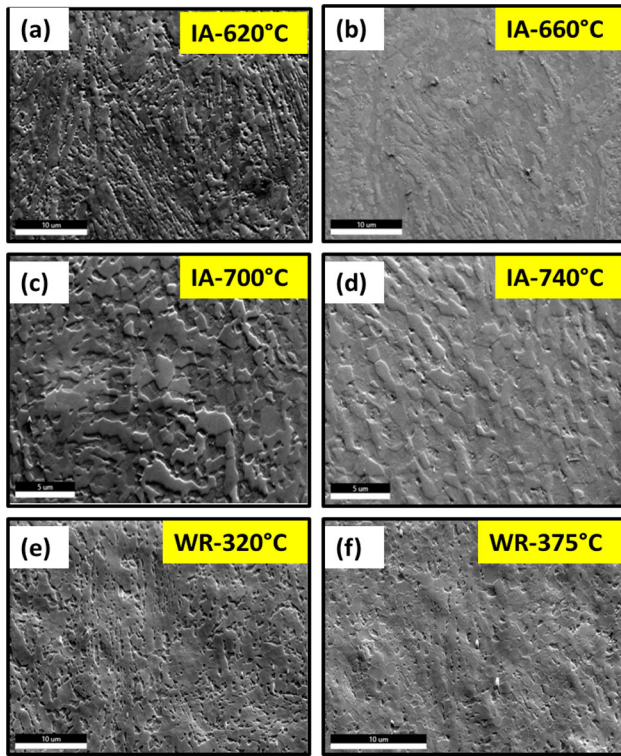


Fig. 6. SEM micrograph of cold-rolled medium-Mn steel under different conditions. (a–d) IA samples; (e–f) IA + WR samples.

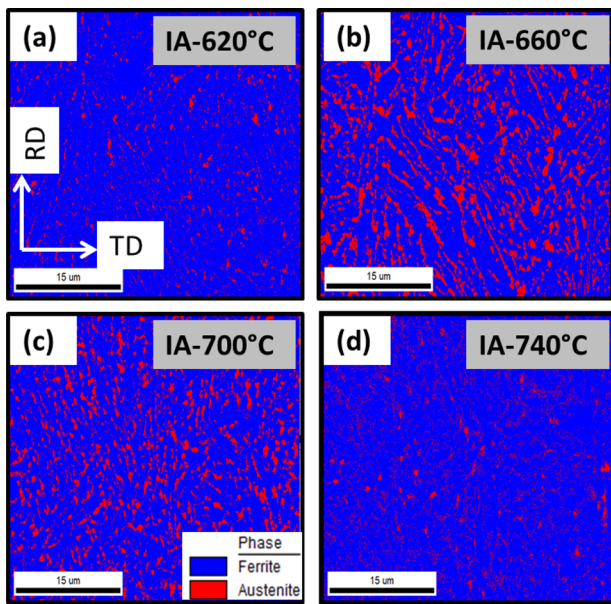


Fig. 7. EBSD phase map of medium-Mn steel annealed at different temperatures for 30 min. The ferrite/martensite phase is indicated in blue, and austenite is indicated in red (Color figure online).

that during intercritical annealing, the volume fraction of retained austenite obtained from XRD and EBSD phase analysis deviates from the predicted one, as shown in Table II. This may be due to the partitioning of C and Mn with increasing

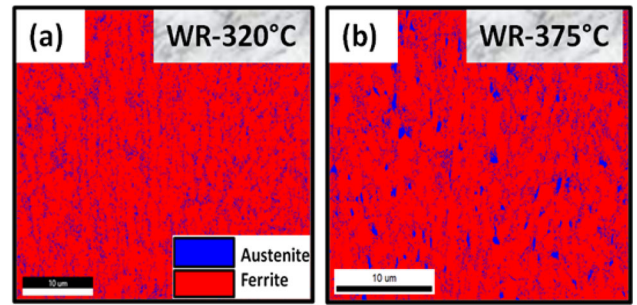


Fig. 8. EBSD phase map of IA + WR samples. Austenite phase is indicated in blue and ferrite/martensite in red (Color figure online).

temperature, but they do not have sufficient time to diffuse into the austenite phase for a holding period of 30 min up to 660°C annealing temperature. With a temperature of 700°C, C and Mn diffuse more rapidly into the austenite phase, improving the austenite formation kinetics and creating an environment in which the austenite can be stabilized with the appropriate amount of C and Mn within 30 min of holding. This may be the reason why the volume fraction of austenite at 700°C is achieved in a higher fraction than the predicted value. In contrast to the EBSD phase map, XRD data show that the maximum volume fraction is obtained at 700°C (around 38.3%). On the other hand, Fig. 10a presents the results of the XRD analysis carried out on the warm-rolled samples. It shows that an increase in the rolling temperature leads to a decrease in the intensity of retained austenite peaks and an increase in the intensity of ferrite peaks. The decrease in the intensity of retained austenite peaks with increasing rolling temperature suggests that the volume fraction of retained austenite decreases at higher rolling temperatures. This can be attributed to the destabilization of the austenite phase under the combined effects of deformation and elevated temperatures during warm rolling. At higher rolling temperatures, the thermodynamic driving force for the austenite-to-ferrite transformation becomes more favorable, leading to a greater extent of austenite decomposition. Additionally, the quantified volume fraction of retained austenite declines steadily with higher rolling temperatures, as shown in Fig. 10b. The steady decrease in the volume fraction of retained austenite with increasing rolling temperature can be attributed to the thermodynamic stability and transformation kinetics of the austenite phase during the warm-rolling process. At higher temperatures, the austenite phase becomes less stable, and its transformation to other phases, primarily ferrite, is thermodynamically favored. As the rolling temperature increases, the diffusion of alloying elements and the mobility of atoms are enhanced, facilitating the transformation kinetics and promoting the decomposition of the metastable austenite phase. In contrast to the EBSD phase map, the XRD data show the

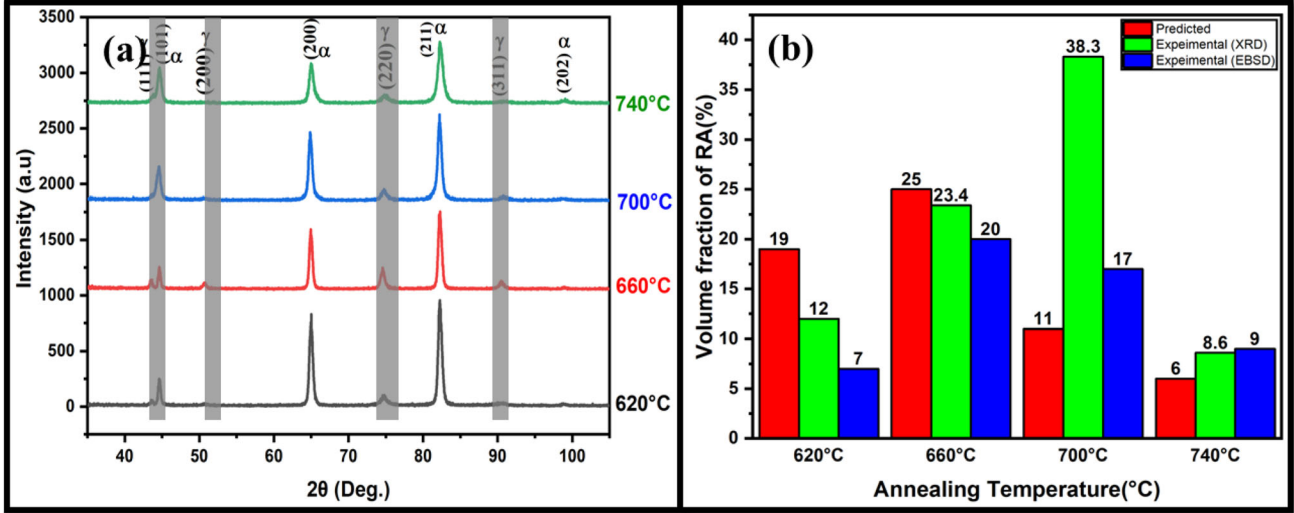


Fig. 9. (a) XRD profiles of the medium-Mn steel after intercritical annealing at temperatures between 620°C and 740°C; (b) amount of retained austenite in the medium-Mn steel dependent on IA temperature.

Table II. Thermo-Calc software predicts the volume fraction of retained austenite, and experimental retained austenite values were calculated by XRD and EBSD phase maps for annealed and warmed samples, respectively

| Temp. (°C) [sample ID] | Heat treatment conditions | Intercritical austenite (vol.%) from thermo-calc | RA obtained by XRD | RA obtained from EBSD phase map |
|---------------------------|--|---|--------------------|---------------------------------|
| IA-620°C | Intercritical annealing at 620°C for 30 min | 18.62 | 12 | 7 |
| IA-660°C | Intercritical annealing at 660°C for 30 min | 25.12 | 23.4 | 20 |
| IA-700°C | Intercritical annealing at 700°C for 30 min | 10.60 | 38.3 | 17 |
| IA-740°C | Intercritical annealing at 740°C for 30 min | 6.05 | 8.6 | 9 |
| WR-320°C | Sample annealed at 660°C for 30 min, then warm rolled after quenching in salt bath maintained at 320° for 80 s | 25.12 | 20.4 | 9 |
| WR-375°C | Sample annealed at 700°C for 30 min, then warm rolled after quenching in salt bath maintained at 375° for 40 s | 10.60 | 15.2 | 9 |

maximum volume fraction obtained at 320°C, as shown in Table II.

Notably, the RA fraction obtained through the EBSD phase map considered a limited area of investigation whereas the one obtained through the XRD analysis considered a definite volume of the sample. Hence, the volume fraction of RA obtained through XRD analysis is statistically robust; therefore, in the rest of this study will discuss the implication of RA fraction on mechanical properties.

Based on XRD analysis, the maximum amount of retained austenite phase is estimated by calculating the integrated intensity of the retained austenite ($I_{\gamma,i}$) and the ferrite ($I_{\alpha,i}$) using Eq. 4¹⁵ as shown in Table II.

$$f_{\gamma} = \frac{\frac{1}{N} \sum_{i=1}^N \left(\frac{I_{\gamma,i}}{R_{\gamma,i}} \right)}{\frac{1}{N} \sum_{i=1}^N \left(\frac{I_{\gamma,i}}{R_{\gamma,i}} \right) + \frac{1}{M} \sum_{j=1}^M \left(\frac{I_{\alpha,j}}{R_{\alpha,j}} \right)} \quad (4)$$

where M and N = numbers of considered retained austenite and ferrite reflections and R = normalization factor corresponding to different phases, which is proportional to the theoretically calculated intensity.

Mechanical Properties

Figure 11a demonstrates the engineering stress-engineering strain curves of the medium-Mn steel Fe-0.2C-5Mn-0.4Al-0.85Si under intercritically annealed conditions and warm-rolled conditions.

Optimizing Microstructure and Mechanical Properties of Cold-Rolled Medium-Mn Steel Through Intercritical Annealing and Warm Rolling

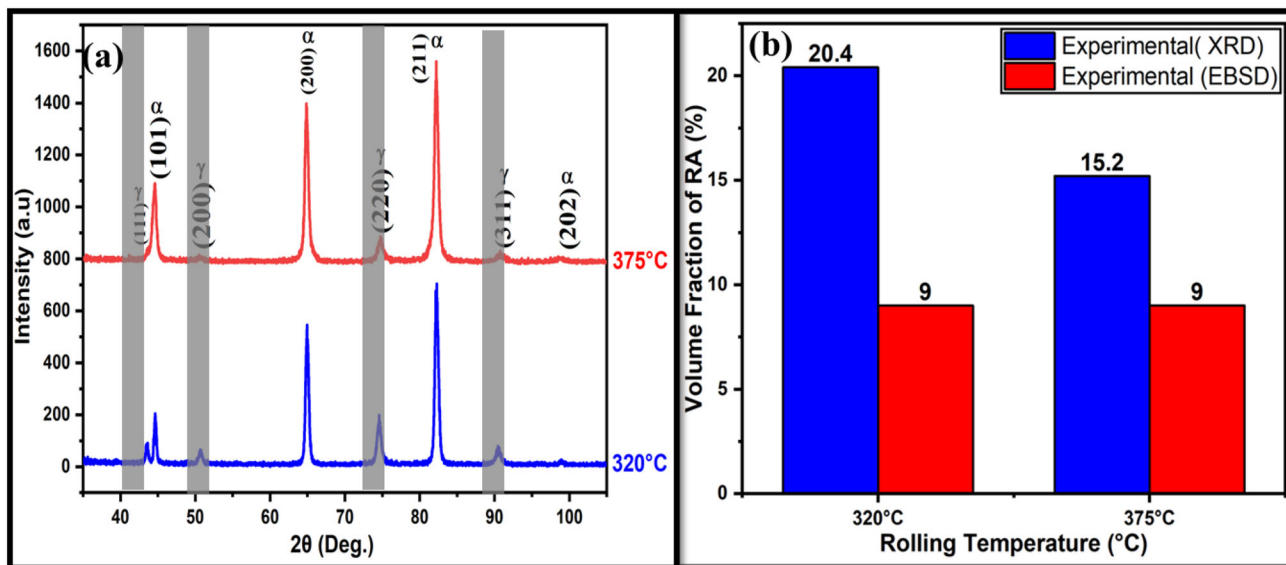


Fig. 10. (a) XRD profiles of the medium-Mn steel after warm rolling at temperatures of 320°C and 375°C; (b) amount of retained austenite in the medium-Mn steel dependent on rolling temperature.

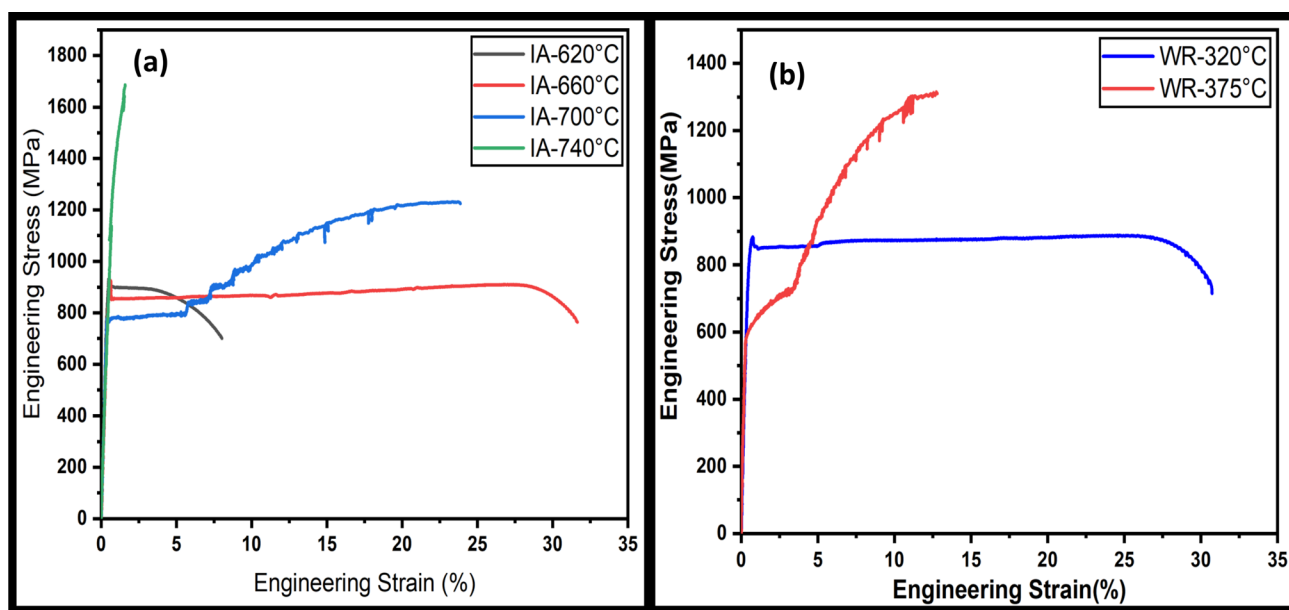


Fig. 11. Engineering stress–strain curves of medium-Mn steel processed by (a) intercritical annealing (IA) at temperature ranging from 620°C to 740°C for 30 min; (b) warm rolling (IA + WR) at start temperature 320°C and 375°C after annealing at 660°C and 700°C for 30 min.

The intercritically annealed samples possessed yield strength (YS) of 858 MPa and ultimate tensile strength (UTS) of 930 MPa, with higher ductility (approximately 32%) at 660°C. This exceptional combination of strength and ductility can be attributed to the favorable microstructure obtained at this annealing temperature, which includes an optimal fraction of retained austenite (RA) and moderate recrystallization. The presence of RA not only contributes to the TRIP (transformation-induced plasticity) effect, enhancing work hardening and strain hardening, but also plays a crucial role in

improving ductility. With an increase in intercritical annealing temperature to 700°C, the sample exhibited a YS of 781 MPa, UTS of 1245 MPa and elongation to break (TE) of 24%, also showing discontinuous yielding behavior with a small amount of localized deformation after yielding. This discontinuous yielding behavior (serration) is mainly attributed to the phenomenon of dynamic strain aging which may be activated after intercritical annealing. Plastic deformation involves the movement of dislocations, causing permanent strain. Solute atoms, such as carbon, segregate

and temporarily pin dislocations, increasing the stress required for further plastic flow. In high-stress situations, dislocations can break free from the solute atmosphere, causing localized strain bursts. It is this cyclic process that leads to stress serration in strain measurements. When the sample was annealed at 740°C, it showed a YS of 1387 MPa and a high UTS (approximately 1685 MPa) but reduced ductility (approximately 2%) due to the mechanical stability of retained austenite being so low that it quickly transformed to martensite at low strain levels. At this higher annealing temperature, the retained austenite becomes less stable, and its rapid transformation to martensite upon deformation leads to a significant increase in strength but compromises the material's ductility.

Figure 11b IA + WR samples showed a YS of 878 MPa, UTS of 888 MPa and TE of 31% after quenching from 660°C. This combination of strength and ductility can be attributed to the optimized microstructure resulting from the intercritical annealing and subsequent warm rolling. The quenching from 660°C likely resulted in the formation of a favorable fraction of retained austenite, which was further stabilized by the holding time of 80 s and the temperature being maintained at 320°C during the salt bath treatment. The presence of retained austenite can contribute to the TRIP (transformation-induced plasticity) effect, enhancing work-hardening behavior and improving the overall ductility through the gradual transformation of austenite to martensite during deformation.

However, when the sample was rolled at 375°C post-quenching from 700°C and held for 40 s, it exhibited a yield strength of 603 MPa, UTS of 1315 MPa and TE of 13%. While the yield strength was lower compared to the samples rolled at 320°C, the ultimate tensile strength was significantly higher, indicating a distinct deformation behavior and work-hardening response. The higher rolling temperature of 375°C and the different holding conditions (post-quenching from 700°C and holding for 40 s) likely influenced the microstructural evolution, phase fractions and stability of retained austenite. The increased ultimate tensile strength observed in the samples rolled at 375°C could be attributed to a higher degree of work hardening or a more favorable distribution and morphology of the retained austenite grains, which can contribute to a more pronounced TRIP effect during deformation. However, the lower yield strength and reduced ductility suggest that the retained austenite may have been less stable or present in a lower fraction, resulting in a different balance between strength and ductility.

In comparison, both IA and IA + WR samples exhibited the presence of Lüders bands during the initial work-hardening stage. The formation of Lüders bands is associated with the dynamic strain aging phenomenon, which occurs because of the interaction between dislocations and solute atoms

or impurities in the material. The warm-rolled condition, however, showed a decrease in Lüders band deformation compared to the IA sample, possibly due to strain-partitioning or the carbon concentration in the ferrite phase. The warm-rolling process can influence the distribution and morphology of the retained austenite grains as well as the partitioning of alloying elements between the different phases, such as austenite, ferrite and martensite. The IA samples displayed a larger yield point elongation associated with Lüders band formation, indicating a more pronounced dynamic strain aging effect in the absence of warm rolling. This observation suggests that the warm-rolling process can potentially mitigate or alter the dynamic strain aging behavior, leading to a reduction in the yield point elongation and Lüders band deformation. The differences in Lüders band behavior between the IA and IA + WR samples can be attributed to the complex interplay among the microstructural features, phase fractions and the deformation mechanisms associated with each processing condition. The warm-rolling step can introduce additional defects, such as dislocations and grain boundaries, which can act as temporary pinning sites for solute atoms or impurities, thereby influencing the dynamic strain aging and Lüders band formation. Furthermore, the warm-rolling process can alter the distribution and morphology of the retained austenite grains, affecting the strain partitioning behavior and the overall deformation mechanisms (Table III).

CONCLUSION

This work investigated the influence of intercritical annealing and warm-rolling parameters on the microstructure and mechanical properties of cold-rolled medium-Mn steel. The following conclusions could be drawn:

1. IA samples exhibit globular morphology of ferrite/martensite and retain austenite after water quenching to room temperature, while IA + WR samples exhibit lamellar morphology of retained austenite and ferrite/martensite when quenched in salt baths at 320°C for 80 s and 375°C for 40 s, respectively, followed by warm rolling.
2. The maximum amount of RA obtained from XRD for the IA samples was 38.3% at 700°C and from EBSD was 17% at 700°C, while at 320°C the maximum amount of RA obtained from XRD for WR samples was 20.4%, while the amount of RA obtained from EBSD was the same at 320°C and 375°C for IA + WR samples.
3. A significant improvement in YS values from 858 MPa to 878 MPa at 320°C and UTS values from 1245 MPa to 1315 MPa at 375°C rolling temperatures is seen after annealing at 660°C and 700°C for 30 min prior to warm rolling.
4. A marginal difference in the total elongation is noticed between the IA and WR samples. At

Table III. Mechanical properties with their standard deviations of IA and IA + WR steel samples under different processing conditions

| Mech. property | IA-620°C | IA-660°C | IA-700°C | IA-740°C | WR-320°C post IA at 660°C | WR-375°C post IA at 700°C |
|---------------------------------|-------------|------------|-------------|--------------|---------------------------|---------------------------|
| Yield strength (MPa) | 903 ± 20.8 | 858 ± 1.44 | 781 ± 4.61 | 1387 | 878 ± 32.3 | 603 ± 9.41 |
| Ultimate tensile strength (MPa) | 931 ± 23.94 | 930 ± 2.72 | 1245 ± 9.53 | 1685 ± 217.1 | 888 ± 22.12 | 1315 ± 8.08 |
| Total elongation (%) | 8 ± 0.95 | 32 ± 0.13 | 24 ± 0.15 | 2 ± 0.55 | 31 ± 3.03 | 13 ± 1.25 |

660°C, the IA samples exhibit a 32% elongation, while the WR samples exhibit a 31% elongation at 320°C with prior annealing at 660°C. Additionally, at 660°C, the IA sample shows a slightly higher combined effect of strength and ductility (29.7%) than the IA + WR sample (which is 27.5 GPa% at 320°C).

- IA samples exhibit yield point elongation, while IA + WR samples also show yielding behavior, albeit less than annealed samples. Warm rolling deforms the material, refines grain size and breaks up coarser carbides, inhibiting dislocation movement, resulting in reduced yielding behavior in IA + WR samples.

Future work should expand the temperature range for warm-rolling experiments, investigate the effect of varying rolling parameters such as reduction ratio, rolling speed and number of passes, evaluate long-term microstructural stability and mechanical properties and optimize warm-rolling process parameters for desired microstructure and mechanical properties. Limitations of the current study include the investigation of a narrow temperature range (320–375°C), the need for a more comprehensive understanding of the underlying mechanisms, insufficient addressing of potential composition-dependent effects and the possibility that laboratory-scale processing may not directly translate to industrial application.

FUNDING

The authors have no relevant financial or non-financial interest to disclose

CONFLICT OF INTEREST

The authors declare that they have no known conflict of interest.

ETHICAL APPROVAL

All authors have followed ethical responsibilities. We confirm that this manuscript submission is original and has not been submitted anywhere for publication.

REFERENCES

- R. Jacob, S.R. Sankaranarayanan, and S.K. Babu, *Mater. Today Proc.* 27, 2852 (2020).
- A. Kozłowska, M. Morawiec, R.H. Petrov, and A. Grajcar, *Mater. Charact.* 199, 112816 (2023).
- R.L. Miller, *Metall. Mater. Trans. B* 3, 905 (1972).
- R. Schneider, K. Steineder, D. Krizan, and C. Sommitsch, *Mater. Sci. Technol.* 35(17), 2045 (2019).
- L. Liu, B. He, and M. Huang, *Adv. Eng. Mater.* 20(6), 1701083 (2018).
- S. Lee, S. Shin, M. Kwon, K. Lee, and B.C. De Cooman, *Metall. Mater. Trans. A* 48, 1678 (2017).
- A. Kapito, R.J. Mostert, W.E. Stumpf, and C.W. Siyasiya, *IOP Conf. Mater. Sci. Eng.* 655(1), 012012 (2019).
- S. Lee and B.C. De Cooman, *Metall. Mater. Trans. A* 45, 6039 (2014).
- Y. Zhang, W. Hui, J. Wang, C. Shao, and X. Zhao, *Steel Res. Int.* 90(3), 1800412 <https://doi.org/10.1002/SRIN.201800412> (2019).
- A.S. Magalhães, C.E. dos Santos, A.O.V. Ferreira, D.S. Alves, and D.B. Santos, *Mater. Sci. Technol.* 35, 2120 (2018).
- E. De Moor, D.K. Matlock, J.G. Speer, and M.J. Merwin, *Scr. Mater.* 64(2), 185 (2011).
- C. Zhao, C. Zhang, W.Q. Cao, and Z.G. Yang, *Int. J. Miner. Metall. Mater.* 23, 161 (2016).
- S. Lee and B.C. De Cooman, *Metall. Mater. Trans. A* 44, 5018 (2013).
- T. Masumura, K. Fujino, T. Tsuchiyama, S. Takaki, and K. Kimura, *ISIJ Int.* 61(2), 546 (2021).
- B.D. Cullity, *Elements of X-Ray Diffraction* (Addison-Wesley Publishing Company Inc, Boston, 1956).

Publisher's Note Springer Nature remains neutral with regard to jurisdictional claims in published maps and institutional affiliations.

Springer Nature or its licensor (e.g. a society or other partner) holds exclusive rights to this article under a publishing agreement with the author(s) or other rightsholder(s); author self-archiving of the accepted manuscript version of this article is solely governed by the terms of such publishing agreement and applicable law.